JCI The Journal of Clinical Investigation

Insulin receptor substrate signaling suppresses neonatal autophagy in the heart

Christian Riehle, … , Morris F. White, E. Dale Abel

J Clin Invest. 2013;123(12):5319-5333. https://doi.org/10.1172/JCI71171.

Research Article **Cardiology**

The induction of autophagy in the mammalian heart during the perinatal period is an essential adaptation required to survive early neonatal starvation; however, the mechanisms that mediate autophagy suppression once feeding is established are not known. Insulin signaling in the heart is transduced via insulin and IGF-1 receptors (IGF-1Rs). We disrupted insulin and IGF-1R signaling by generating mice with combined cardiomyocyte-specific deletion of *Irs1* and *Irs2*. Here we show that loss of IRS signaling prevented the physiological suppression of autophagy that normally parallels the postnatal increase in circulating insulin. This resulted in unrestrained autophagy in cardiomyocytes, which contributed to myocyte loss, heart failure, and premature death. This process was ameliorated either by activation of mTOR with aa supplementation or by genetic suppression of autophagic activation. Loss of IRS1 and IRS2 signaling also increased apoptosis and precipitated mitochondrial dysfunction, which were not reduced when autophagic flux was normalized. Together, these data indicate that in addition to prosurvival signaling, insulin action in early life mediates the physiological postnatal suppression of autophagy, thereby linking nutrient sensing to postnatal cardiac development.

Insulin receptor substrate signaling suppresses neonatal autophagy in the heart

Christian Riehle,[1] Adam R. Wende,[1] Sandra Sena,[1] Karla Maria Pires,[1] Renata Oliveira Pereira,[1] Yi Zhu,[1] Heiko Bugger,[1] Deborah Frank,[1] Jack Bevins,[1] Dong Chen,[2] Cynthia N. Perry,[3] Xiaocheng C. Dong,[4] Steven Valdez,[1] Monika Rech,[1] Xiaoming Sheng,[5] Bart C. Weimer,[2] Roberta A. Gottlieb,[3] Morris F. White,[4] and E. Dale Abel[1]

[1]Division of Endocrinology, Metabolism and Diabetes, and Program in Molecular Medicine, University of Utah School of Medicine, Salt Lake City, Utah, USA. [2]Department of Nutrition and Food Sciences and Center for Integrated BioSystems, Utah State University, Logan, Utah, USA. [3]BioScience Center, San Diego State University, San Diego, California, USA. [4]Division of Endocrinology, Children's Hospital Boston, Harvard Medical School, Boston, Massachusetts, USA. [5]Department of Pediatrics, University of Utah School of Medicine, Salt Lake City, Utah, USA.

The induction of autophagy in the mammalian heart during the perinatal period is an essential adaptation required to survive early neonatal starvation; however, the mechanisms that mediate autophagy suppression once feeding is established are not known. Insulin signaling in the heart is transduced via insulin and IGF-1 receptors (IGF-1Rs). We disrupted insulin and IGF-1R signaling by generating mice with combined cardiomyocyte-specific deletion of *Irs1* and *Irs2*. Here we show that loss of IRS signaling prevented the physiological suppression of autophagy that normally parallels the postnatal increase in circulating insulin. This resulted in unrestrained autophagy in cardiomyocytes, which contributed to myocyte loss, heart failure, and premature death. This process was ameliorated either by activation of mTOR with aa supplementation or by genetic suppression of autophagic activation. Loss of IRS1 and IRS2 signaling also increased apoptosis and precipitated mitochondrial dysfunction, which were not reduced when autophagic flux was normalized. Together, these data indicate that in addition to prosurvival signaling, insulin action in early life mediates the physiological postnatal suppression of autophagy, thereby linking nutrient sensing to postnatal cardiac development.

Introduction

Autophagy is a conserved cellular process that is activated under conditions of nutrient stress to promote cell survival. However, excessive and long-term induction of autophagy may ultimately lead to destruction of essential proteins and organelles, which, beyond a certain threshold, results in cell death (1–3). Constitutive levels of autophagy are low during embryogenesis, but are significantly induced after birth. Myocardial autophagy reaches a maximum at 3–6 hours after birth and maintains organ function in the postnatal starvation period until a consistent nutrient supply is restored via the maternal milk supply (4, 5) and insulin levels rise. However, the underlying mechanisms for the decline in autophagy once feeding is established are incompletely understood. During late gestation, glucose and insulin levels are higher than adult levels, and aas are abundant, which parallels low rates of autophagy (4). Immediately after birth, serum levels of glucagon increase and insulin levels fall (6, 7), in concert with a rapid decline of glucose and aa concentrations (8–10).

Cardiac insulin signaling is transduced via insulin and IGF-1 receptors (IGF-1Rs) (11), which phosphorylate IRSs. IRS proteins bind to PI3K, resulting in the generation of the lipid product PIP_3 and activation of the kinase AKT. AKT orchestrates diverse effects by phosphorylating proteins involved in glycogen synthesis, inhibition of apoptosis, and regulation of gene expression. In addition, AKT mediates the phosphorylation of mechanistic target of rapamycin (mTOR), thereby controlling cellular growth and protein translation via S6 kinase and 4E-BP1 (12). mTOR consists of 2 distinct complexes, mTORC1 and mTORC2. mTOR signaling suppresses autophagy in the presence of nutrients and growth factors (13), and the mTOR inhibitor rapamycin induces autophagy (14). Studies in cell culture models identified the RAGA–RAGD family of GTPases as aa sensors for mTORC1 (15, 16). Mice expressing a constitutively active form of RAGA ($RAGA^{GTP}$), which prevents the inhibition of mTORC1 under conditions of nutrient starvation during the postnatal starvation period, fail to induce autophagy, resulting in accelerated neonatal death (17).

6 members of the IRS family have been identified (18–22). IRS1 and IRS2 are widely expressed, whereas IRS3 is largely restricted to adipose tissue (23). Expression of IRS4 is limited to kidney, brain, thymus, and possibly pancreatic β cells (24). Studies in transgenic mice revealed differential roles for IRS1 and IRS2 signaling in nutrient homeostasis and somatic growth (25). Mice with germline deletion of *Irs1* exhibit a 40%–50% reduction in body weight (26, 27) and a directly proportional reduction in heart weight (28). *Irs2* germline knockout mice have nearly normal birth size and body weight (29). $Irs2^{-/-}$ mice exhibit peripheral insulin resistance and progress toward type 2 diabetes because of pancreatic β cell failure. Furthermore, decreased IRS2 protein levels resulted in increased autophagy in the brain and attenuated the progress of Huntington's disease in a transgenic mouse model by decreasing the number of protein aggregates (30). Together, these studies suggest a predominant role for IRS1 in the regulation of somatic growth and for IRS2 in the regulation of metabolism (26–29).

Given the importance of the insulin/IGF-1/mTOR signaling pathway in the suppression of autophagy and the decrease of postnatal autophagy once feeding is established and insulin levels rise, we sought to test the hypothesis that an important action of insulin in the perinatal period is suppression of postnatal autophagy in the heart. Therefore, we disrupted insulin and IGF-1R signaling by combined cardiomyocyte-specific deletion of *Irs1* and *Irs2*.

Conflict of interest: The authors have declared that no conflict of interest exists.
Citation for this article: *J Clin Invest.* 2013;123(12):5319–5333. doi:10.1172/JCI71171.

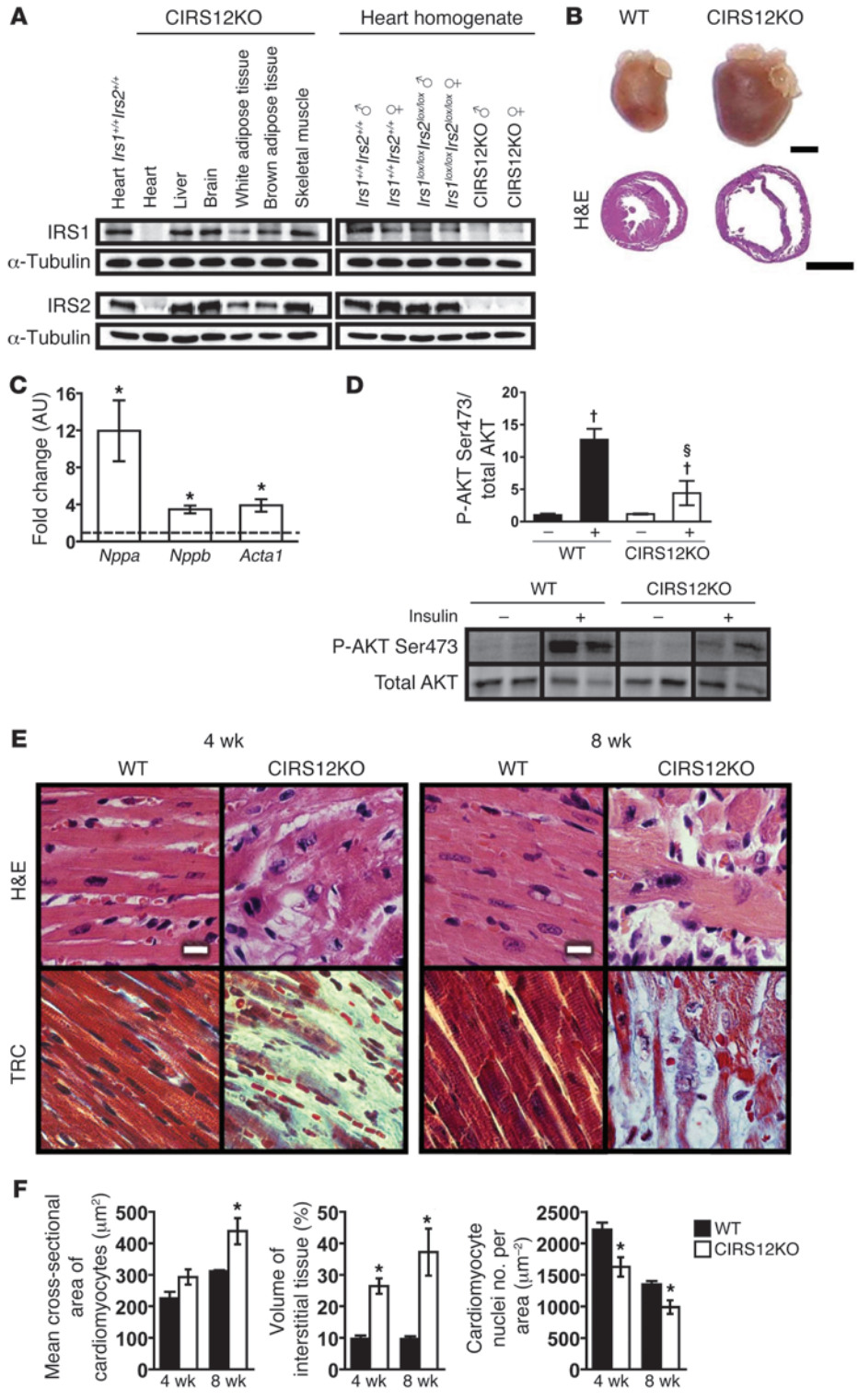

Figure 1
Impaired insulin-mediated signaling and loss of cardiomyocytes in CIRS12KO hearts. (**A**) Representative immunoblots for IRS1 and IRS2 in homogenates of various tissues from 4-week-old CIRS12KO mice and ventricle homogenates from mice with genotypes as indicated. (**B**) Representative photographs and H&E-stained sections from WT and CIRS12KO hearts (4 weeks of age). Scale bars: 2 mm. (**C**) Increased mRNA expression of heart failure/hypertrophy markers in CIRS12KO mice at 4 weeks of age ($n = 8$). Data are expressed as fold change compared with WT (assigned as 1.0; dashed line) and normalized to *Cphn*. (**D**) Phosphorylation of AKT^{Ser473} in ventricle homogenates from 4-week-old CIRS12KO mice was repressed compared with WT controls after injection of 0.01 U insulin into the inferior vena cava. Lanes were run on the same gel but were noncontiguous. (**E** and **F**) Representative H&E and trichrome (TRC) stains (**E**) and stereological analysis (**F**; $n = 3$–6). Scale bars: 10 μm. *$P < 0.05$ vs. WT same age, unpaired Student's t test; §$P < 0.05$ vs. WT same concentration, †$P < 0.05$ vs. same genotype no insulin, ANOVA with Fisher's PLSD.

Results

Impaired insulin-mediated signaling and mitochondrial dysfunction precedes age-dependent contractile dysfunction in CIRS12KO hearts. Cardiomyocyte-specific deletion of both IRS1 and IRS2 proteins was confirmed by immunoblotting in 4-week-old mice (Figure 1A). These CIRS12KO mouse hearts developed dilated cardiomyopathy and showed increased expression of hypertrophy markers (Figure 1, B and C, and Supplemental Figure 1; supplemental material available online with this article; doi:10.1172/JCI71171DS1). Basal levels of AKT^{Ser473} phosphorylation in CIRS12KO hearts were similar to WT controls in 4-week-old mice. However, insulin-stimulated AKT^{Ser473} phosphorylation was impaired by 65.2% compared with

WT controls ($P < 0.05$; Figure 1D). Histology revealed age-dependent myofibrillar loss and disarray and increased fibrosis (Figure 1, E and F). To determine when loss of IRS1 and IRS2 induced cardiac dysfunction, we examined CIRS12KO hearts immediately after birth. Both IRS isoforms were absent in CIRS12KO hearts isolated from these 1-day-old mice (Figure 2A). However, light microscopy revealed normal gross cardiac histology and no increase in fibrotic tissue (Figure 2B). Cardiac function was preserved, and mRNA expression of heart failure/hypertrophy markers was not changed, at 1 day of age (Figure 2, C and D, and Supplemental Table 1). Phosphorylation of insulin-activated targets such as AKT^{Ser473}, $S6^{Ser235/236}$, and $mTOR^{Ser2448}$ was reduced by 74.7%–95.8% ($P < 0.05$). Levels of the γ-band of 4E-BP1 (corresponding to the phosphorylated moiety) were reduced by 51% (Figure 2E), raising the possibility that global protein synthesis could be impaired in CIRS12KO hearts.

We monitored a cohort of CIRS12KO mice and WT littermate controls starting at birth. All CIRS12KO animals died by the age of 11 weeks, with the majority dying by 8 weeks (Figure 2F). Transthoracic echocardiography revealed age-dependent impairment of contractile function and LV dilation (Figure 2G and Supplemental Tables 1 and 2). Transcriptional analysis in 1-day-old hearts showed preserved expression of genes involved in fatty acid oxidation (FAO), oxidative phosphorylation (OXPHOS), and their transcriptional regulators *Ppargc1a* and *Ppargc1b* (encoding PGC-1α and PGC-1β, respectively; Figure 2H). However, at 4 weeks of age, when contractile function was markedly impaired, expression of FAO and OXPHOS genes was repressed by 27.6%–61.5%, in concert with repressed *Ppargc1a* and *Ppargc1b* expression (47.5% and 32.7% reduction, respectively, $P < 0.05$; Figure 2H). Furthermore, analysis of the mitochondrial proteome revealed reduced content of proteins involved in the tricarboxylic acid (TCA) cycle and in fatty acid metabolism (Supplemental Tables 3 and 4). Importantly, expression of genes involved in OXPHOS and FAO was decreased by up to 50% at 2 weeks of age, at a time when cardiac contractile function was preserved. Saponin-permeabilized cardiac fibers were then used to assess mitochondrial function. Fibers obtained from CIRS12KO hearts revealed impaired succinate-supported ADP-stimulated mitochondrial oxygen consumption (V_{ADP}) and ATP production at 2 weeks of age (36.2% and 35.1% reduction, respectively; $P < 0.05$ for each; Figure 2I). Similarly, V_{ADP} and ATP synthesis were decreased by 32.7%–41.1% at 4 weeks of age using pyruvate, palmitoyl-carnitine, or glutamate as substrates ($P < 0.05$ for each; Figure 2J). ATP/O ratios were not changed at either time point (data not shown), suggestive of preserved mitochondrial coupling. Thus, mitochondrial dysfunction clearly precedes the onset of contractile dysfunction and may contribute to heart failure in CIRS12KO mice.

IRS signaling suppresses postnatal autophagy in the heart. Cell death, estimated by the ratio of TUNEL-positive to total nuclei, was maximally increased in 1-day-old CIRS12KO hearts, but declined as animals aged (Figure 3, A and B). Autophagosome content, quantified by cadaverine fluorescence, was increased by 63% in CIRS12KO hearts at 1 day of age ($P < 0.05$) and remained increased by 35% ($P = 0.053$) at 4 weeks of age (Figure 3C). In addition, levels of the proapoptotic proteins cleaved PARP and cleaved caspase-12 were increased, whereas expression of the antiapoptotic protein BCL2 was decreased, consistent with increased apoptotic cell death signaling. LC3-II/LC3-I ratio, assessed by immunoblotting, increased 7.4-fold at 1 day of age. This was paralleled by a 23% increase in protein levels of cathepsin D and a 28.3% reduction in p62 protein levels (Figure 3D), providing additional evidence for increased autophagy in CIRS12KO hearts. ULK1 phosphorylation at the mTOR-dependent Ser757 site was reduced in CIRS12KO hearts (Figure 3D) and has previously been suggested to mediate mTOR-dependent repression of autophagy induction (31). Knockout of *Irs1* and *Irs2* resulted in a mobility shift of ULK1, which was also observed after phosphatase treatment of WT controls (Figure 3D), further supporting impaired ULK1 phosphorylation in CIRS12KO hearts. Interestingly, phosphorylation of $FoxO1^{Thr24}$ and $FoxO3^{Thr32}$ was preserved, and no differences in the phosphorylation of $AMPK^{Thr172}$ and of the AMPK downstream target acetyl-CoA carboxylase at Ser79 (ACC^{Ser79}) were observed (Figure 3D). Electron micrographs prepared from 1-day-old CIRS12KO hearts showed increased numbers of autophagic vesicles (Figure 3E). Expression of genes involved in autophagy regulation and cell death was largely unchanged (Figure 3F). Thus, regulatory mechanisms downstream of mTOR may account for the increase in autophagy and progressive cell loss in CIRS12KO hearts.

To understand potential mechanisms that may induce neonatal autophagy and to explore potential mechanisms for autophagy repression after the establishment of feeding, we examined autophagy levels in WT and CIRS12KO mice in the perinatal time period and correlated these with changes in circulating concentrations of glucose, insulin, and aas. Loss of both IRS isoforms was confirmed in CIRS12KO hearts at E19.5 (Supplemental Figure 2). At 3 hours after Caesarean section, insulin and aa concentrations fell more than 75%, and glucose concentrations by 30%, in mice of all genotypes; these increased with feeding at 3 days (Figure 4, A–C). Autophagy levels were low in cardiac tissue obtained from E19.5 mice immediately after Caesarian section and increased equivalently in WT and CIRS12KO hearts 3 hours after Caesarean section (Figure 4D), which suggests that autophagy induction might be independent of falling insulin concentrations. Although insulin, glucose, and aa concentrations increased in 3-day-old mice, autophagy declined in WT mice, but remained elevated in CIRS12KO mouse hearts (Figure 4, A–D). Milk was found in the stomachs of all mice sacrificed at 3 days. Importantly, CIRS12KO hearts exhibited impaired insulin-mediated signaling, both under basal conditions at 1 day of age and after insulin stimulation (Figure 1D and Figure 2E). Thus, we conclude that IRS signaling mediates the physiological suppression of postnatal autophagy when feeding is established and insulin levels rise. Moreover, the rising circulating concentrations of glucose and aas that correlate with the suppression of perinatal cardiomyocyte autophagy and may contribute to autophagy suppression might be insufficient in the absence of IRS signaling.

Decreased autophagy and attenuated LV remodeling and heart failure in CIRS12KO hearts by aa treatment. To test the hypothesis that decreased mTOR signaling could account for increased autophagy leading to heart failure, we hyperactivated mTOR with aas to determine whether this would be sufficient to inhibit autophagy and prevent heart failure. Branched-chain aas (BCaas) and arginine are powerful activators of mTOR and p70 S6 kinase (S6K1) signaling (32, 33). Thus, we restored mTOR activity in CIRS12KO hearts to levels of WT controls by daily intraperitoneal administration of a BCaa/arginine solution starting at the day of birth. This time point was chosen because we observed the highest rates of autophagy and cell death that also preceded gross changes in cardiac structure and function. Metabolomic analysis confirmed

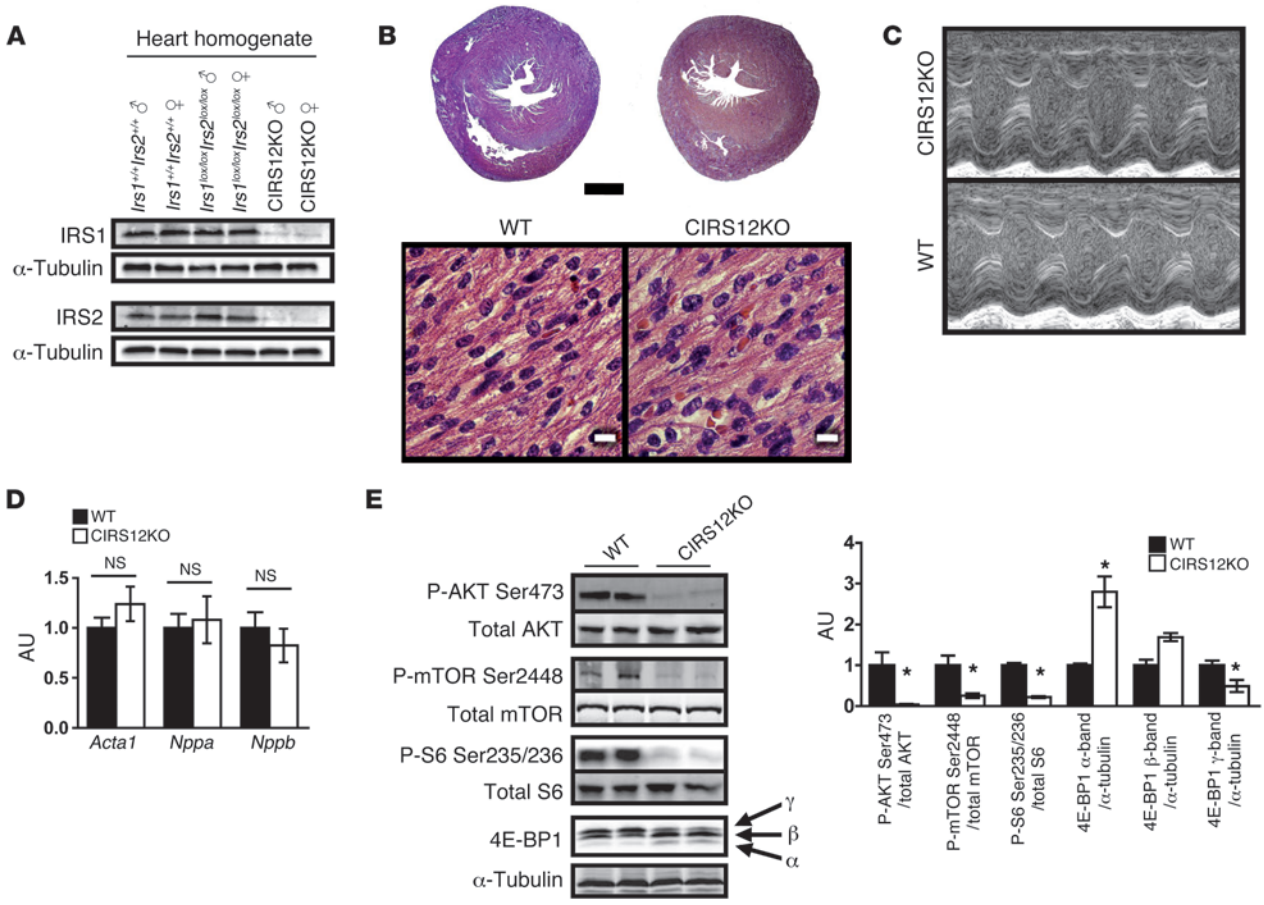
A
Heart homogenate
Irs1+/+Irs2+/+ ♂
Irs1+/+Irs2+/+ ♀
Irs1loxloxIrs2loxlox ♂
Irs1loxloxIrs2loxlox ♀
CIRS12KO ♂
CIRS12KO ♀
IRS1
α-Tubulin
IRS2
α-Tubulin
B
WT
CIRS12KO
C
CIRS12KO
WT
D
WT
CIRS12KO
NS
NS
NS
AU
Acta1
Nppa
Nppb
E
WT
CIRS12KO
P-AKT Ser473
Total AKT
P-mTOR Ser2448
Total mTOR
P-S6 Ser235/236
Total S6
4E-BP1
α-Tubulin
γ
β
α
AU
P-AKT Ser473 /total AKT
P-mTOR Ser2448 /total mTOR
P-S6 Ser235/236 /total S6
4E-BP1 α-band /α-tubulin
4E-BP1 β-band /α-tubulin
4E-BP1 γ-band /α-tubulin
F
Survival (%)
WT (n = 6)
CIRS12KO (n = 8)
P = 0.0003
Log-rank test
Time (wk)
G
FS (%)
1 d
2 wk
4 wk
LVDs (mm)
WT
CIRS12KO
H
Fold change (AU)
Ppargc1a
Ppargc1b
Ppara
Tfam
Nrf1
Nrf2
Ndufv1
Uqcrc1
Cox5b
Acadm
Acadl
Cpt1b
Hadha
Hadhb
Pdk4
Pdha1
Transcriptional regulation
OXPHOS
FAO
Glucose oxidation
CIRS12KO, 1 d
CIRS12KO, 2 wk
CIRS12KO, 4 wk
I
2 wk
VADP (nmol O2/ min/mg dw)
ATP synthesis (nmol/min/mg dw)
Suc
J
4 wk
VADP (nmol O2/ min/mg dw)
ATP synthesis (nmol/min/mg dw)
Pyr
PC
Glu
WT
CIRS12KO

Figure 2
Mitochondrial dysfunction precedes age-dependent contractile dysfunction in CIRS12KO hearts. (**A**) Representative immunoblots for IRS1 and IRS2 in ventricle homogenates obtained from 1-day-old mice. (**B**) H&E stains of 2 chamber sections and higher-magnification views of ventricle sections at 1 day of age. Scale bars: 500 μm (top); 10 μm (bottom). (**C** and **D**) Representative M-mode images showing normal contractile function in CIRS12KO mice (**C**) and mRNA expression of heart failure/hypertrophy markers (**D**) at 1 day of age. (**E**) Diminished phosphorylation of IRS1/IRS2 downstream targets in 1-day-old CIRS12KO hearts. (**F**) Survival curves. (**G**) Time course for FS and LVDs (n = 4–15). (**H**) Age-dependent repression of mRNAs encoding genes involved in FAO and glucose oxidation, OXPHOS, and their transcriptional regulators in CIRS12KO hearts (n = 6–8). Data are presented as fold change compared with same-age WT (assigned as 1.0; dashed line) and normalized to *Cphn* (1 day and 4 weeks) or *Lama1* (2 weeks). (**I**) V_{ADP} and ATP production in cardiac fibers from 2-week-old CIRS12KO mice with succinate (Suc) as substrate plus rotenone (n = 6). dw, dry weight. (**J**) V_{ADP} respiration and ATP synthesis with pyruvate (Pyr), palmitoyl-carnitine (PC), or glutamate (Glu), each combined with malate as substrate in fibers obtained at 4 weeks of age (n = 6). *P < 0.05 vs. WT same age, unpaired Student's t test. See Supplemental Table 11 for gene names.

increased BCaa/arginine levels in serum and heart tissue compared with saline-treated controls (data not shown). Compared with saline-treated controls, aa supplementation attenuated LV dilation and significantly increased the average lifespan of CIRS12KO mice from 6.6 to 11.1 weeks (Figure 5, A and B). Since heart failure per se may independently modulate signal transduction pathways and autophagy, we examined signaling in 2-week-old mice, because contractile function was preserved in CIRS12KO hearts at this age (Figure 2G and Supplemental Table 1).

Autophagic flux was determined by LC3 immunoblotting after injection of the antimalarial drug chloroquine, which neutralizes lysosomal pH and impairs autophagosome fusion with lysosomes. Thus, increased LC3-II accumulation after chloroquine injection is indicative of increased autophagic flux (34). After chloroquine injection, we observed an 8.94-fold increase in the LC3-II/LC3-I ratio in saline-treated CIRS12KO versus WT mice. This effect was attenuated by aa treatment in CIRS12KO animals (79.6% reduction, P < 0.05; Figure 5C). The pathological increase in both heart weight and wet lung weight (pulmonary congestion) was prevented by 6 weeks of aa treatment (Figure 5, D and E, and Supplemental Table 5), consistent with reversal of heart failure. Stereological analysis at 6 weeks of age showed reduced cell loss and replacement fibrosis in CIRS12KO hearts after aa treatment relative to saline-treated controls (Figure 5, F and G). Moreover, transthoracic echocardiography revealed attenuated LV dilation and partial restoration of contractile function (Figure 5H and Supplemental Table 6).

A general linear model was used to compare the adjusted least square mean values of LV cavity diameter at systole (LVDs) and fractional shortening (FS). LVDs in week 4 was significantly lower than week 6 (0.265 vs. 0.308 cm, P < 0.001). In week 4, mean LVDs in aa-treated CIRS12KO mice (0.256 cm) was lower than that in saline-treated CIRS12KO mice (0.310 cm, P < 0.001), and not significantly different from WT controls (0.247 cm, P = 0.414), whereas in week 6, mean LVDs in aa-treated CIRS12KO mice (0.321 cm) was lower than that in saline-treated CIRS12KO mice (0.370 cm, P = 0.007), but higher than WT controls (0.270 cm, P = 0.001). There was no significant difference in mean FS between weeks 4 and 6 (24.27% vs. 22.75%, P = 0.086). Mean FS in aa-treated CIRS12KO mice (20.76%) was higher than that in saline-treated CIRS12KO mice (16.97%, P = 0.001); however, it was lower than WT controls (26.75%, P < 0.001; Figure 5H and Supplemental Table 6). LV catheterization revealed a significant increase in LV developed pressure (34.7% increase) and in maximal rates of dP/dt increase and decrease (65.5% and 73.1%, respectively, P < 0.05 for each) in 6-week-old CIRS12KO mice after aa treatment compared with saline (Figure 5I). Moreover, the increase in LV minimum pressure was completely prevented (Figure 5I and Supplemental Table 7). Thus, aa supplementation attenuated heart failure in CIRS12KO hearts.

Importantly, when contractile function was preserved in CIRS12KO mice by aa treatment, phosphorylation of mTOR^{Ser2448}, S6$^{Ser235/236}$, and ULK1^{Ser757} was restored to the physiological range observed in saline-treated 2-week-old WT mice (Figure 6, A and B). Levels of the antiapoptotic protein BCL2 was decreased and levels of the proapoptotic proteins caspase-8 and cleaved caspase-9 were increased and were not changed after aa supplementation.

Prior studies suggest that BCaa supplementation may increase mitochondrial biogenesis and PGC-1α expression in cardiomyocytes (35). However, aa treatment did not increase the expression levels of *Ppargc1a*, *Ppargc1b*, or their transcriptional targets that regulate mitochondrial OXPHOS or FAO (Supplemental Figure 3). Compared with saline-treated controls, aa supplementation in WT mice had no effect on contractile function, heart weight, apoptotic cell death, glucose tolerance, insulin tolerance, and serum insulin levels after long-term treatment for 20 weeks (Supplemental Methods and Supplemental Figures 4 and 5).

Mitochondrial dysfunction persists in CIRS12KO hearts after aa treatment and normalization of autophagic flux. Protein levels of OXPHOS subunits were reduced in parallel with decreased activity of the mitochondrial enzymes citrate synthase (CS) and hydroxyacyl-CoA dehydrogenase (HADH) in CIRS12KO hearts (Figure 7, A–C). Similarly, V_{ADP} and ATP production, as assessed in saponin-permeabilized cardiac fibers, were decreased in CIRS12KO hearts (Figure 7, D and E). None of these defects were reversed by aa supplementation (Figure 7, A–E). Together, these data support the hypothesis that aa supplementation suppresses autophagy, but has no effect on apoptotic cell death and mitochondrial dysfunction, in CIRS12KO hearts.

Heterozygous deletion of Becn1 decreases autophagy and attenuates contractile dysfunction in CIRS12KO hearts. To independently confirm that decreasing autophagy is necessary and sufficient to reverse heart failure in CIRS12KO hearts, we reduced autophagy levels in CIRS12KO hearts by crossing them with mice that are haploinsufficient for *Becn1* (referred to herein as CIRS12KO×*Becn1*$^{+/-}$ mice; see Methods). BECN1 is required for autophagosome formation, and heterozygous deletion of *Becn1* decreases autophagy (36). Similar to aa treatment, heterozygous *Becn1* deletion decreased autophagic flux in the CIRS12KO×*Becn1*$^{+/-}$ hearts to levels observed in WT controls at 2 weeks of age and extended lifespan. Normalizing autophagy prevented the increase in heart and lung weight, reduced LV dilation, improved contractile function, and decreased cardiomyocyte loss and replacement fibrosis at 6 weeks of age (Figure 8, A–I, and Supplemental Tables 8–10). A general linear model with Tukey-Kramer multiple comparison adjustment was used to compare the adjusted least square mean values of LVDs and FS. Mean LVDs in week 4 was significantly lower than in week 6 (0.254 vs. 0.291 cm, P < 0.001). Mean LVDs was statistically lower in CIRS12KO×*Becn1*$^{+/-}$ mice (0.274 cm) than CIRS12KO mice (0.322 cm, P < 0.001), although it was still

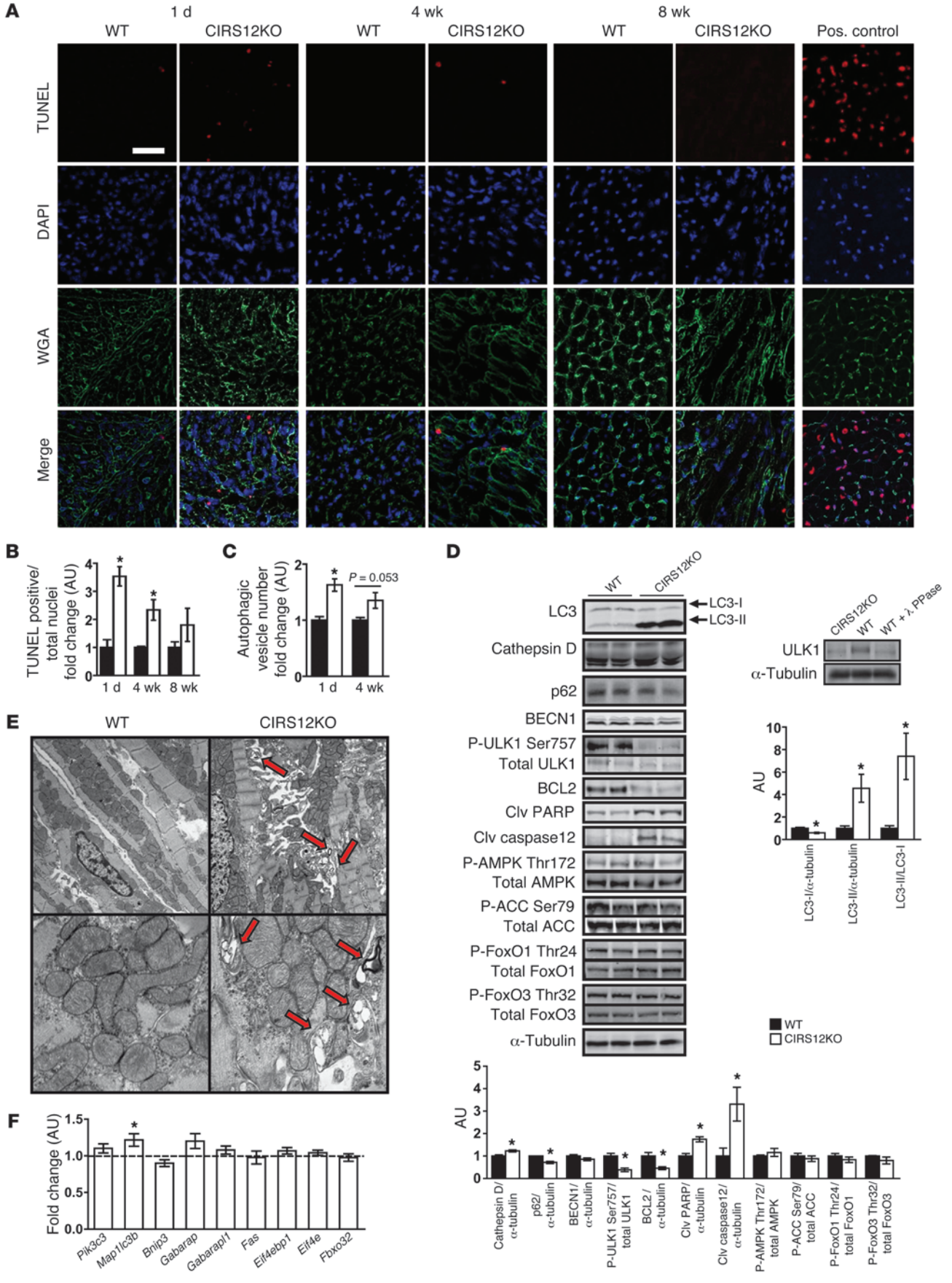
A
1 d
4 wk
8 wk
WT
CIRS12KO
WT
CIRS12KO
WT
CIRS12KO
Pos. control
TUNEL
DAPI
WGA
Merge
B
TUNEL positive/ total nuclei fold change (AU)
1 d
4 wk
8 wk
C
Autophagic vesicle number fold change (AU)
P = 0.053
1 d
4 wk
D
WT
CIRS12KO
LC3
LC3-I
LC3-II
Cathepsin D
p62
BECN1
P-ULK1 Ser757
Total ULK1
BCL2
Clv PARP
Clv caspase12
P-AMPK Thr172
Total AMPK
P-ACC Ser79
Total ACC
P-FoxO1 Thr24
Total FoxO1
P-FoxO3 Thr32
Total FoxO3
α-Tubulin
CIRS12KO
WT
WT + λ PPase
ULK1
α-Tubulin
AU
LC3-I/α-tubulin
LC3-II/α-tubulin
LC3-II/LC3-I
WT
CIRS12KO
AU
Cathepsin D/ α-tubulin
p62/ α-tubulin
BECN1/ α-tubulin
P-ULK1 Ser757/ total ULK1
BCL2 / α-tubulin
Clv PARP/ α-tubulin
Clv caspase12/ α-tubulin
P-AMPK Thr172/ total AMPK
P-ACC Ser79/ total ACC
P-FoxO1 Thr24/ total FoxO1
P-FoxO3 Thr32/ total FoxO3
E
WT
CIRS12KO
F
Fold change (AU)
Pik3c3
Map1lc3b
Bnip3
Gabarap
Gabarapl1
Fas
Eif4ebp1
Eif4e
Fbxo32

Figure 3
Increased autophagy and apoptosis in CIRS12KO hearts. (**A**) Representative TUNEL, DAPI, and wheat germ agglutinin (WGA) staining and (**B**) stereological quantification (n = 3–4). Scale bar: 20 μm. (**C**) Autophagy quantified by cadaverine fluorescence staining of autophagosomes was increased by 63% and 35% at 1 day and 4 weeks of age, respectively (n = 6). (**D**) Representative Western blots and densitometric quantification for proteins involved in autophagy regulation and cell survival at 1 day of age (n = 3–6). Knockout of *Irs1* and *Irs2* resulted in a mobility shift of ULK1, which was also observed after phosphatase treatment of WT control, suggestive of impaired ULK1 phosphorylation in CIRS12KO hearts. (**E**) Representative electron micrographs from CIRS12KO and WT controls at 1 day of age showing increased formation of autophagosomes (arrows) in CIRS12KO hearts. Original magnification, ×5,000 (top); ×20,000 (bottom). (**F**) mRNA levels of genes involved in autophagy regulation and cell survival in 1-day-old CIRS12KO hearts (n = 6). Data are presented as fold change versus age-matched WT control (assigned as 1.0; dashed line) and normalized to *Cphn*. *P < 0.05 vs. WT same time point, unpaired Student's t test. See Supplemental Table 11 for gene names.

higher than *Becn1*$^{+/-}$ (0.249 cm, P = 0.037) and WT (0.245 cm, P = 0.010) controls. Mean FS in week 4 was not statistically different from week 6 (26.25% vs. 24.69%, P = 0.161). Mean FS in CIRS12KO×*Becn1*$^{+/-}$ mice (24.81%) was statistically higher than CIRS12KO mice (18.96%, P < 0.001), although it was still lower than *Becn1*$^{+/-}$ (28.79%, P = 0.025) and WT (29.32%, P = 0.003) controls (Figure 8H and Supplemental Table 10). Echocardiographic findings were supported by LV catheterization that revealed near-normalization of LV developed pressures and *dP/dt* in 6-week-old mice (Figure 8I and Supplemental Table 9). Western blot analysis at the 2-week time point revealed reduced mTOR signaling, increased levels of the proapoptotic proteins caspase-8 and cleaved caspase-9, and reduced abundance of the antiapoptotic protein BCL2 that persisted after heterozygous deletion of *Becn1* (Figure 9, A and B).

Mitochondrial dysfunction persists in CIRS12KO hearts after heterozygous deletion of Becn1 and normalization of autophagic flux. Similar to our results with aa supplementation, CIRS12KO×*Becn1*$^{+/-}$ mice exhibited decreased OXPHOS protein content and mitochondrial dysfunction (Figure 10, A–E). Furthermore, mRNA expression levels of *Ppargc1a* and genes involved in FAO and OXPHOS were reduced (Figure 10F). Thus, despite increased survival and delayed heart failure onset, heart failure eventually developed in CIRS12KO animals when the overactivation of autophagy was prevented. Therefore, additional mechanisms arising from reduced insulin signaling, such as mitochondrial dysfunction and increased apoptosis that were not affected by aa supplementation or heterozygous deletion of *Becn1*, contribute to the development of heart failure in CIRS12KO hearts.

Discussion

The present study revealed that loss of *Irs1* and *Irs2* in cardiomyocytes led to heart failure that was multifactorial in nature, resulting from increased autophagy, increased apoptosis, and mitochondrial dysfunction. The rapid evolution of cardiomyocyte dysfunction provided a challenge to elucidating the inciting and proximal mechanisms for the changes observed. For this reason, we performed a careful analysis of potential pathophysiological mechanisms beginning at 1 day of age and subsequently at 2 and then 4 weeks. Given our observation that autophagic flux was increased at the earliest time point examined, prior to repression of transcripts that regulate nuclear-encoded mitochondrial genes and before structural and functional changes developed, we focused our investigation on testing the novel hypothesis that insulin signaling may represent the critical mediator of the suppression of perinatal cardiac autophagy once feeding is established. We used 2 independent approaches to suppress autophagy in CIRS12KO hearts. Activation of mTOR signaling by aa supplementation or heterozygous deletion of *Becn1* decreased autophagic flux in CIRS12KO hearts to levels observed in WT controls. This delayed the onset of heart failure and prolonged the lifespan of CIRS12KO mice. However, normalization of autophagy did not prevent the increase in apoptosis or mitochondrial dysfunction. Together, these data support an essential role for insulin signaling in the physiological regulation of perinatal cardiac autophagy after the onset of feeding, which contributes in part to the pathophysiology of heart failure in CIRS12KO mice.

Earlier studies by our group confirmed that insulin and IGF-1Rs can efficiently transduce insulin signaling in cardiomyocytes (11), which may explain why deletion of insulin receptors and IGF-1Rs do not result in catastrophic phenotypes (37–39). Deletion of *Irs1* and *Irs2* in cardiomyocytes using the α*MHC* promoter led to near-complete abrogation of insulin signal transduction at 1 day of age. Notably, there was a significant repression in mTOR signaling and dephosphorylation of ULK1, which likely accounts for the persistent activation of autophagy in this model. IRS1 and IRS2 are ubiquitously expressed, and we believe that persistent expression of IRS1 and IRS2 in nonmyocytes such as fibroblasts account for residual insulin signaling that was more evident in 4-week-old CIRS12KO hearts, which were characterized by increased fibrosis. Although CIRS12KO cardiomyocytes were refractory to insulin signaling, we cannot rule out a role for a defect in IGF-1 signaling in suppressing neonatal autophagy, given recent observations suggesting that IGF-1 signaling may partially mediate starvation-induced autophagy in cardiomyocytes (40).

We observed increased levels of proapoptotic proteins and repression of the antiapoptotic protein BCL2 that persisted when autophagic flux was normalized by either aa supplementation or heterozygous deletion of *Becn1*. Therefore, increased apoptosis likely represents an independent mechanism contributing to increased cell death in CIRS12KO hearts that is independent of autophagic flux. Growth factor signaling is a well-established regulator of apoptosis acting via PI3K and AKT signaling pathways, which were constitutively repressed in CIRS12KO hearts. Crosstalk between apoptotic and autophagic signaling has been well described (40). That the persistence of apoptotic signaling after autophagy was repressed by either aa-mediated mTOR activation or reducing *Becn1* supports the hypothesis that IRS1 and IRS2 signaling may regulate these cell death pathways via distinct mechanisms.

The present study confirmed an important role for insulin signaling in the regulation of mitochondrial function and oxidative capacity. We previously reported in mice with cardiomyocyte-specific deletion of insulin receptors (CIRKO mice) that mitochondrial bioenergetics was impaired on the basis of reduced expression of mitochondrial proteins involved in the TCA cycle and FAO. These changes were associated with increased oxidative stress, mitochondrial uncoupling, and an age-dependent defect in ATP production and oxygen consumption (39). However, in contrast to CIRS12KO hearts, CIRKO hearts did not develop a spontaneous cardiomyopathy. Interestingly, deletion of IGF-1Rs

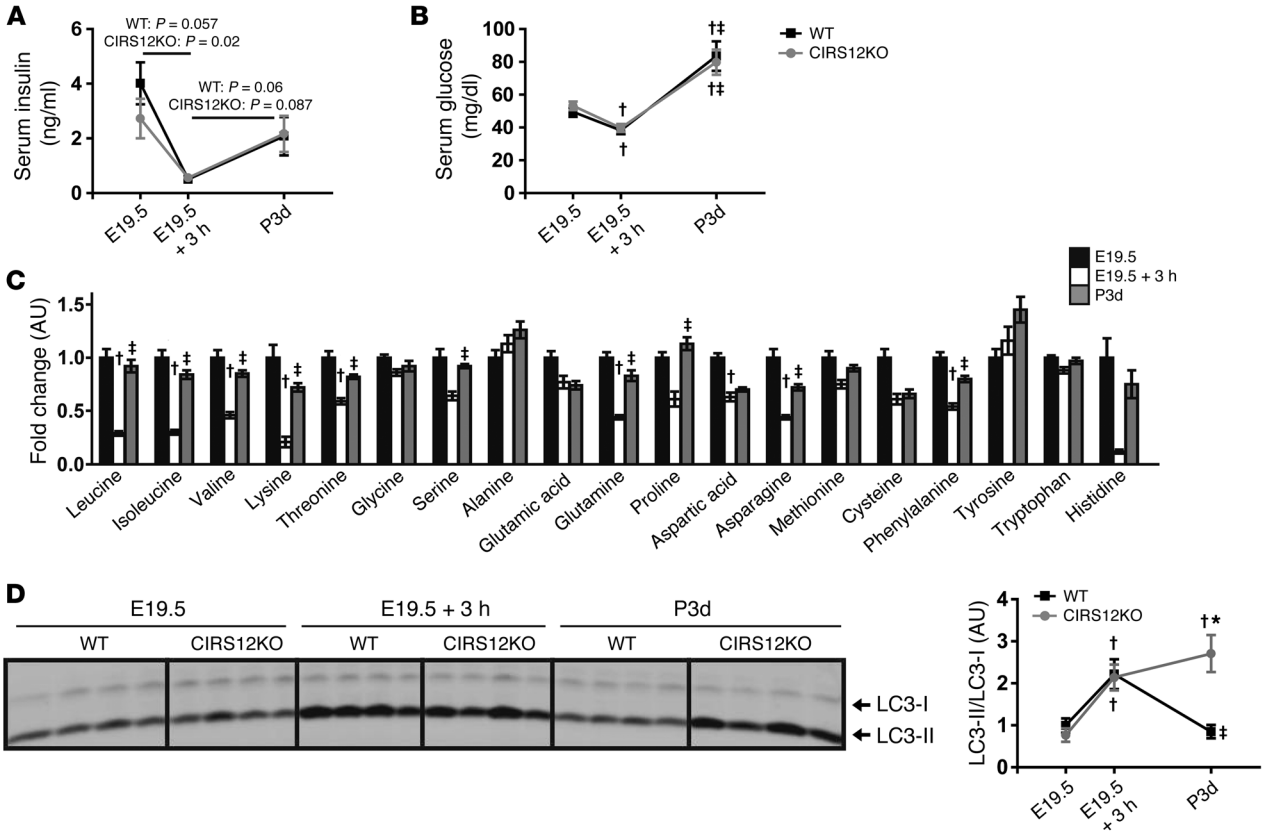

Figure 4
IRS signaling suppresses postnatal autophagy. (**A**–**D**) Time course of (**A**) serum insulin and (**B**) serum glucose in WT and CIRS12KO mice, (**C**) serum aa levels in WT mice, and (**D**) autophagy, as assessed by LC3-II/LC3-I immunoblotting, in WT and CIRS12KO mouse hearts. Newborn mice were obtained by Caesarean delivery at E19.5. Pups were either immediately sacrificed or placed in a humidified, temperature-controlled chamber for 3 hours before sacrifice (E19.5 + 3h). For the 3-day time point (P3d), pups were removed from mothers 3 days after natural birth and immediately sacrificed. *$P < 0.05$ vs. WT same time point, †$P < 0.05$ vs. E19.5 same genotype, ‡$P < 0.05$ vs. E19.5 + 3h same genotype, unpaired Student's *t* test.

in cardiomyocytes was not associated with any baseline defects in mitochondrial bioenergetics (38). Thus, the more severe mitochondrial phenotype of CIRS12KO mouse hearts likely reflects a more profound defect in insulin signaling that was offset by a modest induction in IGF-1R expression in CIRKO hearts, which retain the ability to respond to insulin (11, 38). A mouse model with combined deficiency of insulin and IGF-1Rs in cardiac and skeletal muscle has also been described. Similar to our CIRS12KO model, these mutant mice developed early-onset dilated cardiomyopathy and died from heart failure within the first month of life (41). This study suggested mitochondrial dysfunction as a cause for heart failure, although analyses were performed at a time when cardiac dysfunction was already present. We also observed mitochondrial dysfunction in CIRS12KO hearts at the age of 2 weeks that was not improved by aa supplementation or heterozygous deletion of *Becn1*. It is important to emphasize that repression of nuclear-encoded genes that regulate mitochondrial metabolism was not present at 1 day of age, at a time when autophagy was increased, but was present at 2 weeks of age and prior to the onset of heart failure. Thus, the impairment of mitochondrial function that is attributable to loss of insulin signaling in cardiomyocytes reflects incompletely understood mechanisms that may govern mitochondrial homeostasis or protein turnover requiring a longer time scale to evolve. Regardless, because mitochondrial dysfunction preceded contractile dysfunction, it is likely to contribute to the onset of heart failure in this model. The changes observed in the mitochondrial proteome and mitochondrial energetics in 4-week-old CIRS12KO mice were more severe than those previously reported in a model of pressure overload–induced heart failure (42). Our present results are therefore consistent with a model in which mitochondrial dysfunction may not only incite heart failure, but progressively becomes further impaired as heart failure ensues.

Earlier studies from our group and others revealed that genetic reduction of mTOR expression in cardiomyocytes resulted in dilated cardiomyopathy and increased mortality (43, 44). In one study, mTOR knockout hearts exhibited accumulation of 4E-BP1, which inhibits translation initiation. Cardiomyocytes obtained from mTOR-knockout hearts showed decreased protein synthesis in vitro, and reducing 4E-BP1 attenuated the heart failure phenotype of mTOR-knockout hearts (43). We also observed reduced phosphorylation of 4E-BP1 in CIRS12KO hearts in parallel with impaired mTOR signaling, which was not affected by heterozygous deletion of *Becn1*. Therefore, the possibility exists that total protein synthesis might be impaired in CIRS12KO

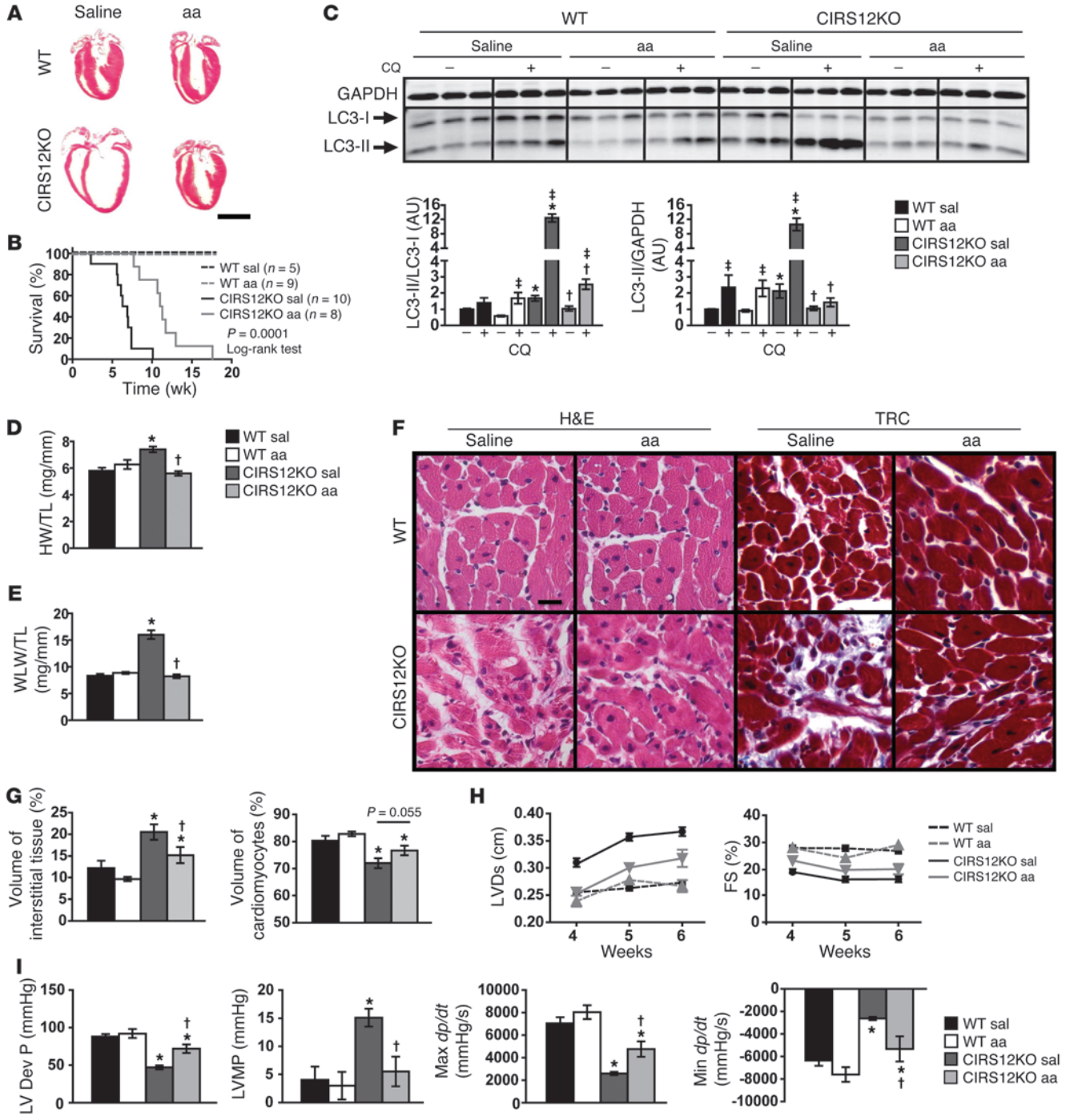

Figure 5

Decreased autophagy and attenuated heart failure by aa treatment in CIRS12KO mice. (**A**) Representative H&E stains from WT and CIRS12KO hearts (6 weeks of age) after saline or aa treatment. Scale bar: 3 mm. (**B**) Survival curves showing that aa supplementation increased the average lifespan of CIRS12KO mice from 6.6 to 11.1 weeks ($P = 0.0001$, log-rank test). (**C**) Autophagy flux after chloroquine (CQ) injection (2 weeks of age), as measured by LC3 immunoblotting. (**D**) Heart weight/tibia length (HW/TL) and (**E**) wet lung weight/tibia length (WLW/TL) ratios after saline or aa treatment in 6-week-old mice. (**F** and **G**) Representative H&E and trichrome staining (**F**) and stereological analysis (**G**; $n = 6–7$). Scale bar: 20 μm. (**H**) Time course for LVDs and FS ($n = 6–9$). (**I**) Invasive measurement of LV pressures in WT and CIRS12KO hearts after saline or aa treatment at 6 weeks of age, as assessed by catheterization. LV Dev P, LV developed pressure; LVMP, LV minimum pressure; Max *dP*/*dt* and Min *dP*/*dt*, maximal rates of increase and decrease, respectively, in LV pressure. *$P < 0.05$ vs. WT same treatment, †$P < 0.05$ vs. saline same genotype, ‡$P < 0.05$ vs. same genotype no chloroquine, ANOVA with Fisher's PLSD.

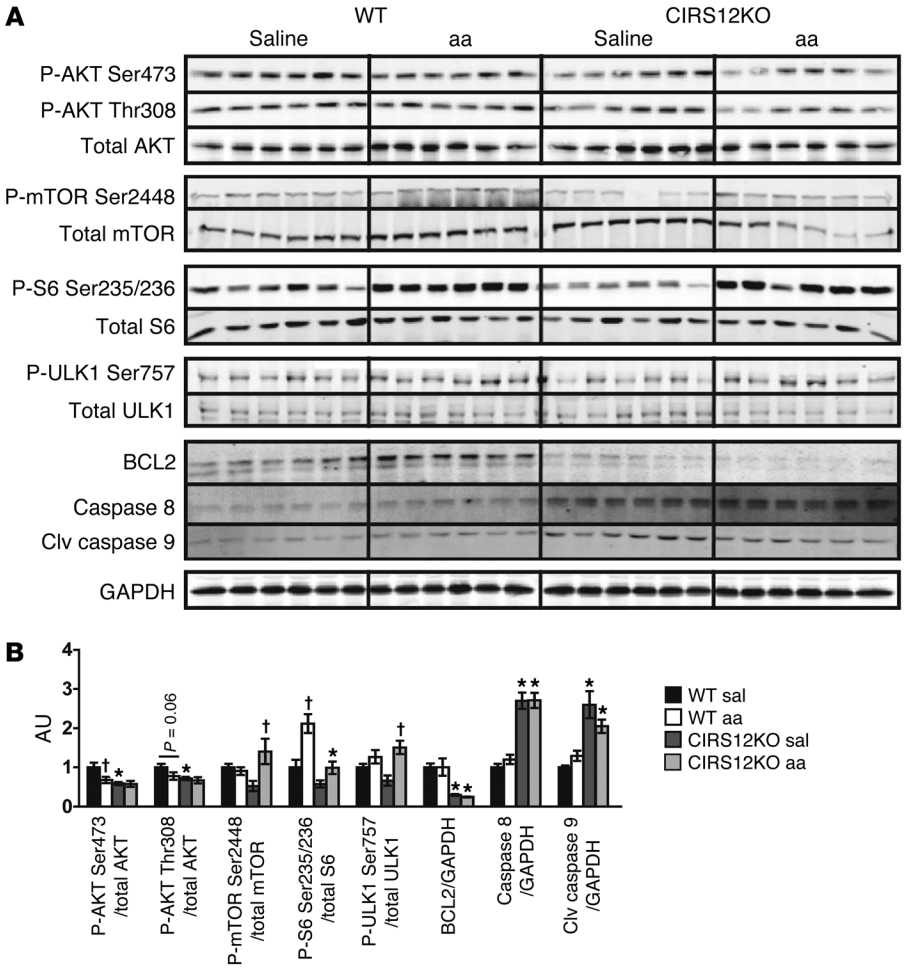

Figure 6
Increased proapoptotic signaling in CIRS12KO hearts persists after aa treatment. Immunoblots (**A**) and quantification (**B**) from ventricle homogenates obtained from CIRS12KO and WT mice after saline or aa treatment at 2 weeks of age. *$P < 0.05$ vs. WT same treatment, †$P < 0.05$ vs. saline same genotype, ANOVA with Fisher's PLSD.

hearts and could represent an additional mechanism contributing to the onset of heart failure in these hearts. In CIRS12KO hearts, aa supplementation restored mTOR signaling to levels observed in WT controls. However, heart failure still ensued after aa supplementation in CIRS12KO hearts. These data suggest that autophagic and apoptotic cell death and mitochondrial dysfunction may play the predominant role in contributing to heart failure onset in CIRS12KO hearts relative to any contribution of impaired protein synthesis.

We used BCaas as a tool to activate mTOR signaling and determine whether suppression of autophagy is sufficient to restore cardiac structure and function in CIRS12KO hearts. In addition to this putative mechanism, it is important to note that BCaas are anaplerotic substrates (45). This raised the possibility that BCaa/arginine supplementation could have contributed to improved cardiac function by providing anaplerotic substrate support. This possibility cannot be formally excluded. However, the persistence of mitochondrial dysfunction after aa treatment — as evidenced by repression of OXPHOS content, reduced mitochondrial enzyme activities, and impaired ATP production with the complex II substrate succinate — suggests that the severity of mitochondrial dysfunction might not have been mitigated by increased anaplerotic support. The role of insulin signaling in the regulation of mitochondrial anaplerosis will be the subject of future investigation.

In conclusion, the present study identified IRS signaling as a critical physiological regulator of cardiomyocyte homeostasis and survival by suppressing apoptosis and autophagy and facilitating the developmental increase in mitochondrial energetic capacity. We focused our investigations primarily on the novel role of insulin signaling in suppressing perinatal cardiac autophagy once feeding is established after birth. The inability to sense nutrients promotes a persistent increase in autophagy that contributes to myocyte loss and heart failure. Thus, insulin/IGF-1 signaling through IRS proteins represents an important mediator of the perinatal adaptation of the heart to nutrient availability and the development of cardiac metabolic pathways, linking nutrient sensing to postnatal cardiac structural and functional maturation.

Methods

Generation of transgenic mouse models. CIRS12KO mice ($Irs1^{lox/lox}Irs2^{lox/lox}$ $\alpha MHC\text{-}Cre^{+/-}$) were generated by breeding $Irs1^{lox/lox}Irs2^{lox/lox}$ with $\alpha MHC\text{-}Cre^{+/-}$ mice, then crossing the resulting $Irs1^{+/lox}Irs2^{+/lox}\alpha MHC\text{-}Cre^{+/-}$ animals with $Irs1^{lox/lox}Irs2^{lox/lox}$ mice. CIRS12KO×$Becn1^{+/-}$ mice were bred in an analogous manner (mice with haploinsufficiency for *Becn1* were provided by B. Levine, University of Texas Southwestern, Dallas, Texas, USA). Generation of transgenic $Irs1^{lox/lox}$, $Irs2^{lox/lox}$, $\alpha MHC\text{-}Cre^{+/-}$, and $Becn1^{+/-}$ mice has been described previously (36, 46–48). WT controls for CIRS12KO harbored homozygous floxed alleles for both *Irs1* and *Irs2* in the absence of $\alpha MHC\text{-}Cre$. Mice expressed both alleles for *Becn1* unless otherwise indicated. Geno-

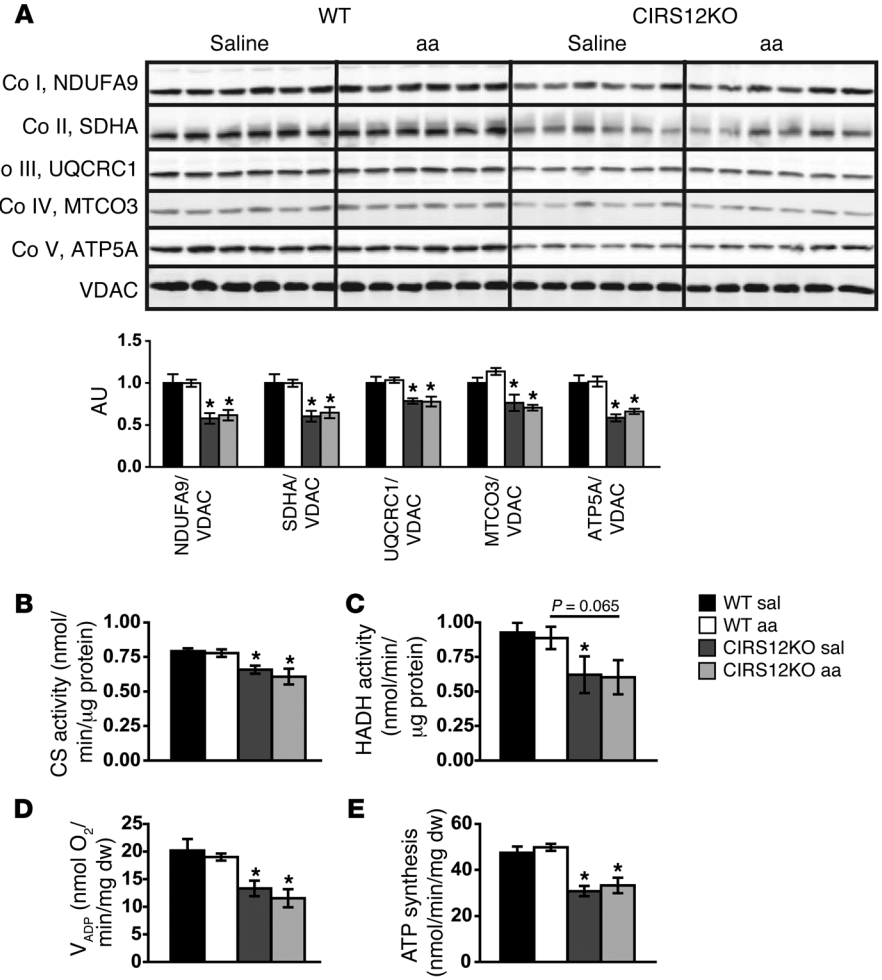

Figure 7
Mitochondrial dysfunction and decreased OXPHOS protein content in CIRS12KO hearts persist after aa treatment. (**A**) Immunoblots for OXPHOS subunits and quantification from ventricle homogenates at 2 weeks of age ($n = 6$). (**B** and **C**) Mitochondrial CS (**B**) and HADH (**C**) activity in CIRS12KO hearts remained reduced after aa treatment ($n = 6$) at 2 weeks of age. (**D** and **E**) Impaired V_{ADP} respiration (**D**) and ATP production (**E**) in cardiac fibers from 2-week-old CIRS12KO mice treated with saline or aa with succinate (as substrate) plus rotenone ($n = 4$–5). *$P < 0.05$ vs. WT same treatment.

typing of mice was performed as previously described (36, 46–48). All mice were maintained on a C57BL/6-129Sv mixed genetic background. Animals were housed with a 12-hour light/12-hour dark cycle at 22°C with free access to food and water. Data shown are from male mice.

RNA extraction and quantitative RT-PCR. Total RNA was extracted from hearts with TRIzol reagent (Invitrogen), purified with the RNeasy kit (Qiagen Inc.), and reverse transcribed. Quantitative real-time PCR was performed using SYBR Green I and ROX internal reference (49). See Supplemental Table 11 for primer sequences and accession numbers.

Evaluation of insulin-stimulated AKT phosphorylation. Mice were anesthetized (single intraperitoneal injection of chloral hydrate, 400 mg/kg body weight) after a 6-hour fast starting at 6AM, and mice were injected with 0.01 U insulin or saline via the inferior vena cava. Hearts were rapidly excised 5 minutes after injection, snap frozen in liquid nitrogen, and processed for Western blot analysis.

Western blot analysis. Total protein extraction was performed as previously reported (50). Proteins were resolved by SDS-PAGE and electrotransferred to nitrocellulose (IRS, P-mTOR/total mTOR, and P-ACC/total ACC) or PVDF membranes (other targets). Primary antibodies against 4E-BP1, NADH dehydrogenase (ubiquinone) 1α, subcomplex 9 (NDUFA9); succinate dehydrogenase complex, subunit A (SDHA); ubiquinol–cytochrome *c* reductase core protein I (UQCRC1); cytochrome *c* oxidase subunit 3 (MTCO3); and ATP synthase, subunit α (ATP5A), were from Abcam. Primary antibody against VDAC was from Thermo Scientific. Primary antibodies against IRS1 and IRS2 were from Millipore. Primary antibodies against LC3 and α-tubulin were from Sigma-Aldrich. Primary antibodies against cathepsin D, p62 (SQSTM1), FoxO3 (FKHRL1), and ULK1 were from Santa Cruz Biotechnology. Primary antibodies against ACC, AKT, AMPKα, Atg7, BECN1, BCL2, caspase-8, cleaved caspase-9, caspase-12, cleaved PARP^{Asp214}, FoxO1, GAPDH, mTOR, P-ACC^{Ser79}, P-AKT^{Ser473}, P-AKT^{Thr308}, P-AMPKα^{Thr172}, P-FoxO1^{Thr24}/FoxO3a^{Thr32}, P-FoxO3a$^{Ser318/321}$, P-mTOR^{Ser2448}, P-S6 ribosomal protein$^{Ser235/236}$, P-ULK1^{Ser555}, P-ULK1^{Ser757}, and S6 ribosomal protein were from Cell Signaling. Protein detection was carried out with the appropriate ho rseradish peroxidase–conjugated secondary antibody/ECL detection systems (Amersham Biosciences) or Alexa Fluor anti-rabbit 680 (Invitrogen) and anti-mouse 800 (VWR International) as secondary antibodies, and fluorescence was quantified using the LI-COR Odyssey imager.

Electron microscopy. LV samples were prepared as previously described (51).

Fluorescence determination of autophagosomes. Autophagosomes were isolated from tissue samples and incubated with the fluorescent cadaverine compound. Fluorescence was read on a plate reader and adjusted by protein concentration of the sample (52).

Histology and stereology. Myocardial fragments were stained with H&E (Fisher), Masson's trichrome (Sigma-Aldrich), TUNEL (Roche), DAPI (Invitrogen), or wheat germ agglutinin (Invitrogen). Stained slides were analyzed with a 36-point test system, and stereology was performed as previously described (53).

Mitochondrial proteome analysis. Mitochondria isolation for mitochondrial proteomic analysis, protein in-solution tryptic digestion, expression

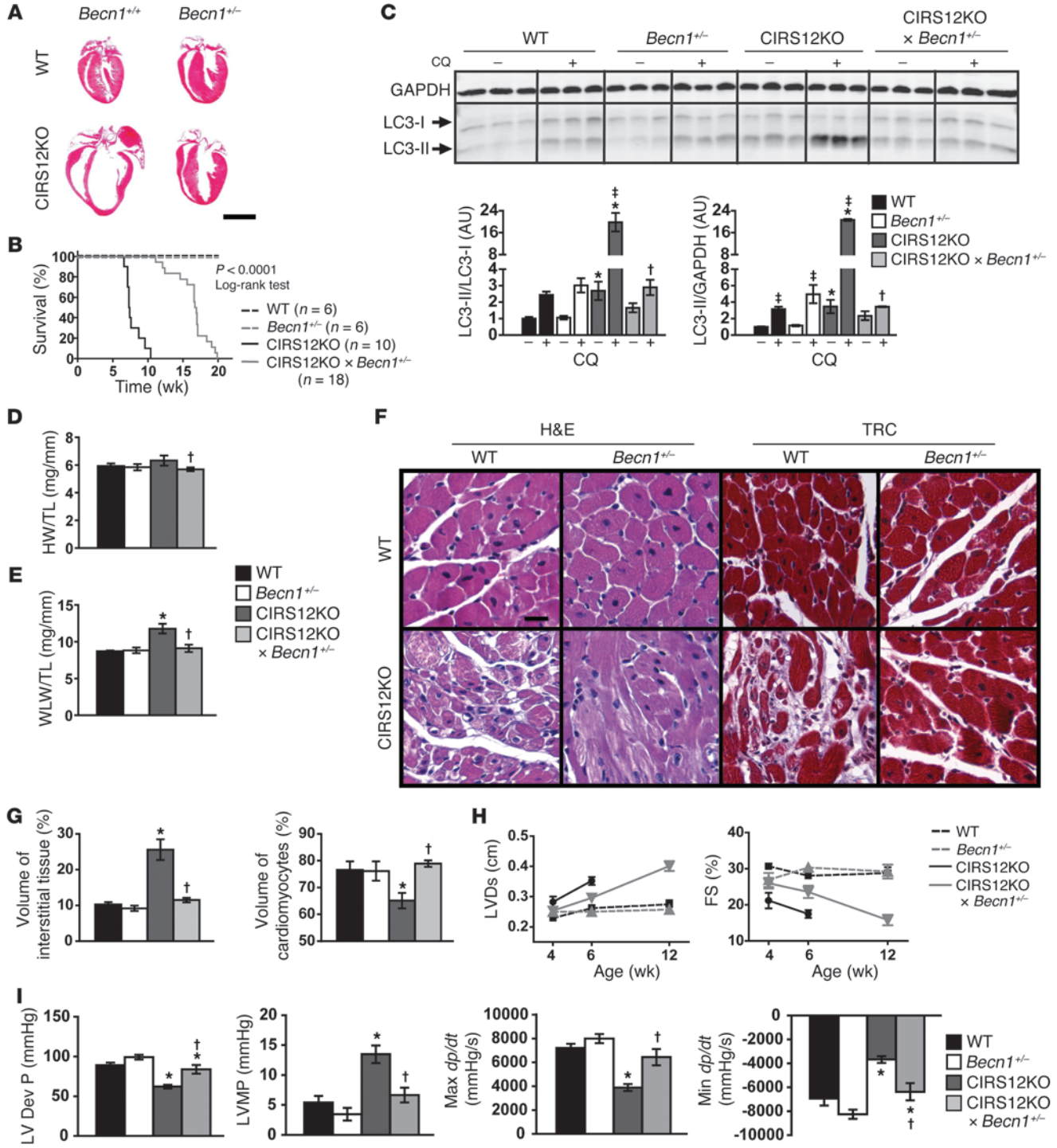

Figure 8

Heterozygous deletion of *Becn1* decreases autophagy and attenuates heart failure in CIRS12KO mice. (**A**) Representative H&E stains from WT and CIRS12KO hearts (6 weeks of age) expressing *Becn1*$^{+/+}$ or *Becn1*$^{+/-}$ alleles. Scale bar: 3 mm. (**B**) Survival curve of WT, *Becn1*$^{+/-}$, CIRS12KO, and CIRS12KO×*Becn1*$^{+/-}$ mice. Heterozygous deletion of *Becn1* increased the average lifespan of CIRS12KO mice from 7.4 to 16.8 weeks ($P < 0.0001$, log-rank test). (**C**) Autophagy flux after chloroquine injection at 2 weeks of age, as measured by LC3 immunoblotting. (**D**) Heart weight/tibia length and (**E**) wet lung weight/tibia length ratios. (**F** and **G**) Representative H&E and trichrome staining (**F**) and stereological analysis (**G**; $n = 6–7$) in hearts from 6-week-old mice. Scale bar: 20 μm. (**H**) Time course for LVDs and FS ($n = 5–10$). (**I**) Invasive measurement of LV pressures in WT and CIRS12KO hearts expressing *Becn1*$^{+/+}$ or *Becn1*$^{+/-}$ alleles at 6 weeks of age, as assessed by catheterization. *$P < 0.05$ vs. same *Becn1* genotype, †$P < 0.05$ vs. same *Irs* genotype, ‡$P < 0.05$ vs. same genotype no chloroquine.

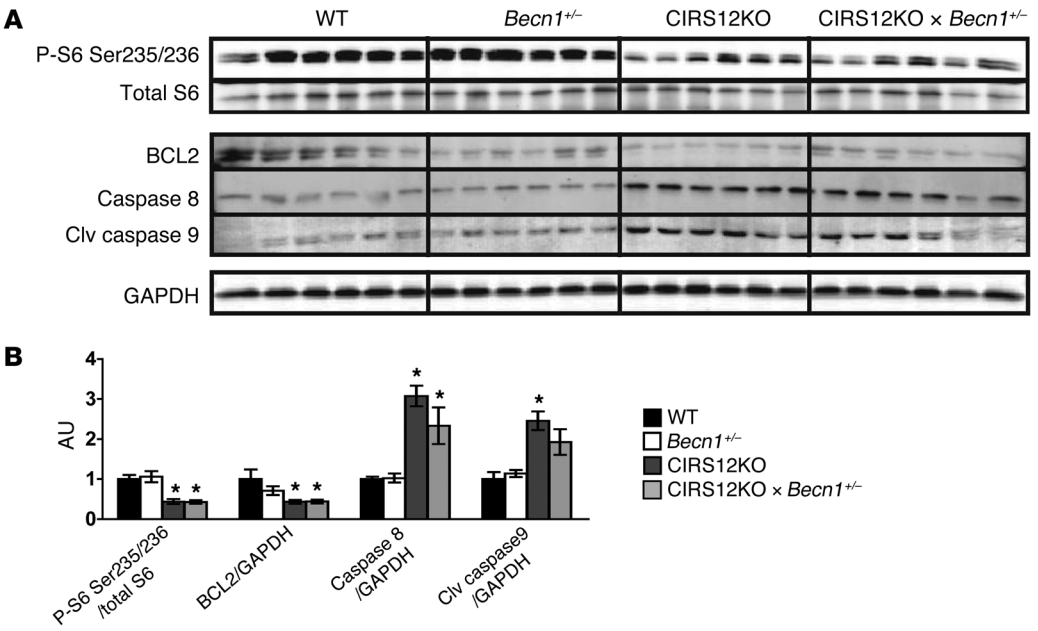

Figure 9
Impaired insulin signaling and increased proapoptotic signaling in CIRS12KO×*Becn1*$^{+/-}$ hearts. Immunoblots (**A**) and quantification (**B**) from ventricle homogenates at 2 weeks of age ($n = 6$). *$P < 0.05$ vs. same *Becn1* genotype.

analysis by mass spectrometry, and statistical analysis of data were performed as previously described (54).

Mitochondrial function in saponin-permeabilized cardiac fibers. LV subendocardial muscle fibers were used to measure mitochondrial respiration rates and ATP synthesis as previously described (55). Respiration rates were determined under 3 different conditions: in the presence of substrate alone (V_O), after stimulation with 1 mM ADP (V_{ADP}), and after addition of 1 μg/ml of the ATP synthase inhibitor oligomycin (V_{Oligo}).

Mitochondrial enzyme activity assays. CS and HADH enzyme activity were determined as previously described (56) using a Synergy HT Multi-Detection Reader (Bio-Tek Instruments) with a total reaction volume of 200 μl.

Transthoracic echocardiography. Mice were anesthetized with isoflurane, and 2-dimensional guided M-mode images were taken in both short- and long-axis projections. A Vevo 660 ultrasound machine (Visualsonics Inc.) with a 40-MHz transducer was used for 1-day and 2-week-old mice; a Vivid 7 Pro ultrasound machine with a 13-Mhz linear probe (GE Medical Systems) was used for the other groups.

Treatment with aa supplementation. Injections of aa solution were performed daily. The aa solution was administered intraperitoneally starting at the day of birth at a dosage of 0.1 ml/g body weight with a maximal dose of 2 ml/d. All aas were purchased from Sigma-Aldrich. The solution contained the following aa concentrations: 6.0 g/l isoleucine, 12.0 g/l leucine, 7.2 g/l valine, and 6.04 g/l arginine (pH 7.4). PBS (pH 7.4; Invitrogen) was used as a control.

Measurement of autophagic flux. CIRS12KO mice, injected with aa solution starting the day of birth, or CIRS12KO×*Becn1*$^{+/-}$ mice were injected with chloroquine (Sigma-Aldrich). The following dose was used: 30 mg/kg body weight 48 hours prior to harvest (at 12 days of age) and 30 mg/kg body weight 24 hours prior to harvest. Mice were sacrificed at 2 weeks of age, after a 6-hour fast starting at 6AM and 2 hours after the final injection of chloroquine (40 mg/kg body weight). Heart tissues were then snap frozen and subjected to immunoblotting analysis.

LV catheterization. A 1.4 F micromanometer-tipped pressure catheter (Millar Instruments) was retrogradely inserted into the LV via the right carotid artery. Hemodynamic measurements were obtained using LabChart7 Pro software (ADInstruments) (55).

Caesarean delivery. Mice were anesthetized (single intraperitoneal injection of chloral hydrate at 400 mg/kg body weight), and Caesarean delivery was performed at E19.5. Pups were either immediately sacrificed or placed in a humidified, temperature-controlled chamber (37°C) for 3 hours before sacrifice. Pups for the 3-day time point (after natural birth) were removed from their mothers and immediately sacrificed. Milk was found in the stomachs of all pups examined at 3 days of age. Blood samples were collected following decapitation, and hearts were snap frozen in liquid nitrogen.

Measurement of serum insulin levels. For the 20-week time point, blood samples were collected by submandibular bleed after a 6-hour fast starting at 6AM. Serum insulin concentrations were measured using a rat insulin RIA kit (Millipore) for 20-week-old mice or using an Ultra Sensitive Rat Insulin ELISA Kit (Chrystal Chem Inc.) for newborn mice.

Metabolomic analysis and measurement of serum aa levels. Tissue and serum were snap frozen in liquid nitrogen and subjected to gas chromatography–mass spectrometry (GC-MS) and liquid chromatography–mass spectrometry (LC-MS). See Supplemental Methods for details.

Statistics. Data are expressed as mean ± SEM. Unpaired 2-tailed Student's *t* test was used to analyze data with 2 groups. For multigroup comparisons, data were analyzed by ANOVA, and significance was assessed by Fisher's protected least significant difference (PLSD) test using StatView 5.0.1 software (SAS Institute). In analyses comparing 2 variables, such as cardiac function in control and knockout mice as a function of age and treatment or genotype, a general linear model (e.g., 2-way ANOVA) was used. When significant differences existed across multiple ages, a Tukey-Kramer multiple-comparison adjustment was performed on post-hoc comparisons to determine at which ages the measures were different (SAS 9.0.3 software; SAS Institute). Proteomic data were analyzed using Waters ProteinLynx

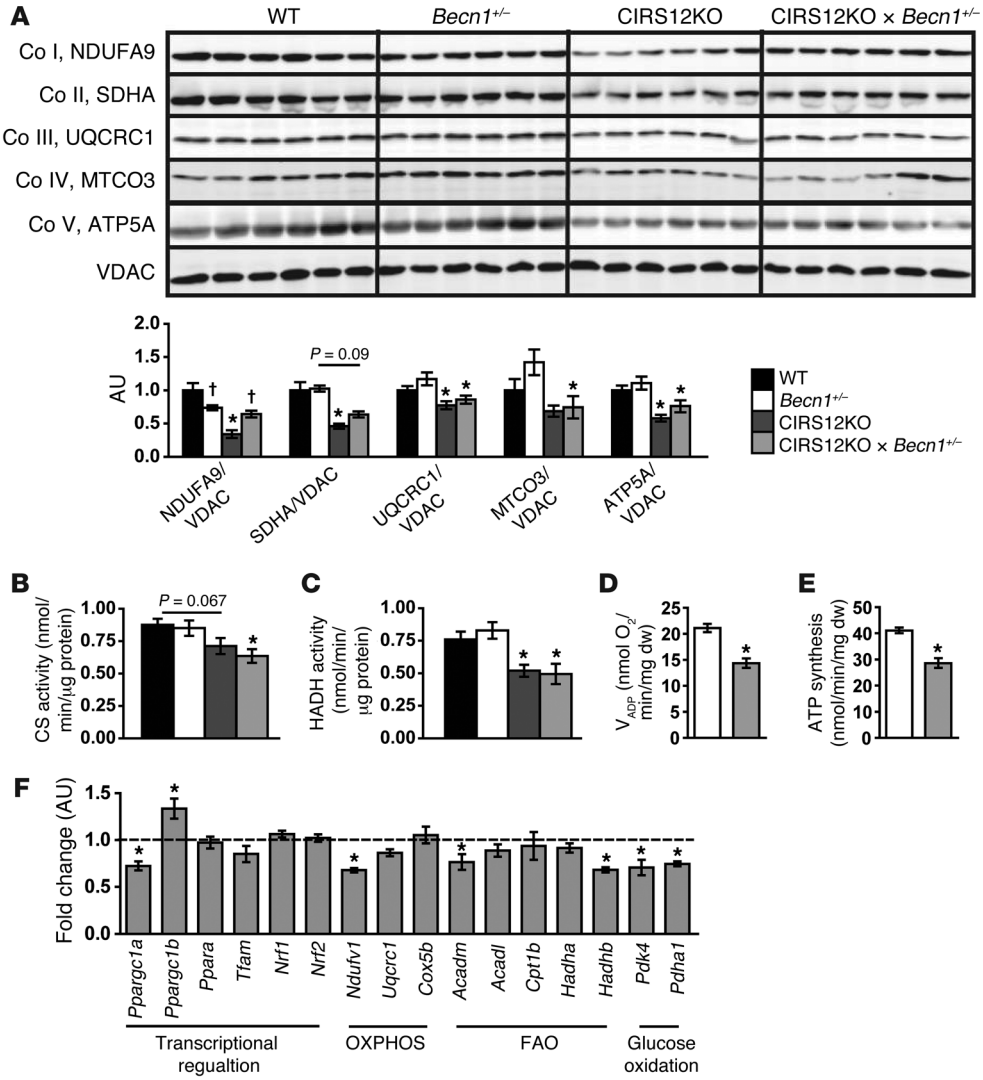

Figure 10
Mitochondrial dysfunction and decreased OXPHOS protein content in CIRS12KO×*Becn1*$^{+/-}$ hearts. (**A**) Immunoblots for OXPHOS subunits and quantification from ventricle homogenates at 2 weeks of age (n = 6). (**B** and **C**) Reduced mitochondrial CS (**B**) and HADH (**C**) activity in CIRS12KO hearts were not rescued in CIRS12KO×*Becn1*$^{+/-}$ hearts (n = 6) at 2 weeks of age. (**D** and **E**) V_{ADP} respiration (**D**) and ATP production (**E**) were reduced in cardiac fibers from 2-week-old CIRS12KO×*Becn1*$^{+/-}$ mice with succinate (as substrate) plus rotenone (n = 6). (**F**) Gene expression in 2-week-old CIRS12KO×*Becn1*$^{+/-}$ hearts (n = 6). Data are presented as fold change versus *Becn1*$^{+/-}$ (assigned as 1.0; dashed line) and normalized to *Gapdh*. $^{*}P < 0.05$ vs. same *Becn1* genotype, $^{\dagger}P < 0.05$ vs. same *lrs* genotype. See Supplemental Table 11 for gene names.

Global Server 2.3 software (Waters) followed by unpaired 2-tailed Student's t tests. For all analyses, a P value less than 0.05 was considered significant.

Study approval. All experiments were performed in accordance with protocols approved by the Institutional Animal Care and Use Committee of the University of Utah.

Acknowledgments

This work was supported by NIH grants RO1DK092065, RO1HL070070, RO1HL108379 UO1HL087947 to E.D. Abel, who is an established investigator of the American Heart Association. C. Riehle was supported by fellowships from the Biomedical Sciences Exchange Program (BMEP) and the Erwin Riesch Foundation and by a postdoctoral fellowship from the German Research Foundation (DFG). A.R. Wende was supported by an advanced postdoctoral fellowship from the JDRF (10-2009-672) and by NIH grant K99 HL111322. K.M. Pires was supported by the Coordenação de Aperfeiçoamento de Pessoal de Nível Superior (CAPES, Brazil). R.O. Pereira was supported by a postdoctoral fellowship from the AHA (Western Affiliates) and by NIH grant T32 HL007576. H. Bugger was supported by a postdoctoral fellowship from the DFG. M. Rech was supported by fellowships from Maastricht University and the Netherlands Heart Foundation (NHF). The authors thank Heather Theobald, Benjamin Wayment, and Curtis Olsen for technical assistance and the laboratory of Beth Levine for providing mice with haploinsufficiency for *Becn1*.

Received for publication May 24, 2013, and accepted in revised form August 29, 2013.

Address correspondence to: E. Dale Abel, Fraternal Order of Eagles Diabetes Research Center and Division of Endocrinology and Metabolism, Roy J. and Lucille A. Carver College of Medicine University of Iowa, 108 CMAB, 451 Newton Road, Iowa City, Iowa 52242, USA. Phone: 319.353.3050; Fax: 319.335.8327; E-mail: DRCAdmin@uiowa.edu.

Sandra Sena's present address is: Université Victor Segalen-Bordeaux 2, Bordeaux, France.

Heiko Bugger's present address is: Department of Cardiology, University of Freiburg, Freiburg, Germany.

Xiaocheng C. Dong's present address is: Department of Biochemistry and Molecular Biology, Indiana University School of Medicine, Indianapolis, Indiana, USA.

Bart C. Weimer's present address is: University of California Davis, School of Veterinary Medicine, Department of Population Health and Reproduction, Davis, California, USA.

1. Gustafsson AB, Gottlieb RA. Recycle or die: the role of autophagy in cardioprotection. *J Mol Cell Cardiol*. 2008;44(4):654–661.
2. Valentim L, et al. Urocortin inhibits Beclin1-mediated autophagic cell death in cardiac myocytes exposed to ischaemia/reperfusion injury. *J Mol Cell Cardiol*. 2006;40(6):846–852.
3. Aki T, Yamaguchi K, Fujimiya T, Mizukami Y. Phosphoinositide 3-kinase accelerates autophagic cell death during glucose deprivation in the rat cardiomyocyte-derived cell line H9c2. *Oncogene*. 2003;22(52):8529–8535.
4. Kuma A, et al. The role of autophagy during the early neonatal starvation period. *Nature*. 2004; 432(7020):1032–1036.
5. Medina G, Vicario C, Juanes M, Fernández E. Biochemical adaptations to early extrauterine life. In: Herrera E, Knopp RH, eds. *Perinatal Biochemistry*. CRC Press: Boca Raton, Florida, USA; 1992:233–258.
6. Girard J, Ferre P, Pegorier JP, Duee PH. Adaptations of glucose and fatty acid metabolism during perinatal period and suckling-weaning transition. *Physiol Rev*. 1992;72(2):507–562.
7. Girard JR, Cuendet GS, Marliss EB, Kervran A, Rieutort M, Assan R. Fuels, hormones, and liver metabolism at term and during the early postnatal period in the rat. *J Clin Invest*. 1973;52(12):3190–3200.
8. Cornblath M, Reisner SH. Blood glucose in the neonate and its clinical significance. *N Engl J Med*. 1965;273(7):378–381.
9. Sperling MA, DeLamater PV, Phelps D, Fiser RH, Oh W, Fisher DA. Spontaneous and amino acid-stimulated glucagon secretion in the immediate postnatal period. Relation to glucose and insulin. *J Clin Invest*. 1974;53(4):1159–1166.
10. Gain KR, Malthus R, Watts C. Glucose homeostasis during the perinatal period in normal rats and rats with a glycogen storage disorder. *J Clin Invest*. 1981;67(5):1569–1573.
11. Ikeda H, et al. Interaction of myocardial insulin receptor and IGF receptor signaling in exercise-induced cardiac hypertrophy. *J Mol Cell Cardiol*. 2009;47(5):664–675.
12. Schmelzle T, Hall MN. TOR, a central controller of cell growth. *Cell*. 2000;103(2):253–262.
13. Levine B, Kroemer G. Autophagy in the pathogenesis of disease. *Cell*. 2008;132(1):27–42.
14. Rubinsztein DC, Gestwicki JE, Murphy LO, Klionsky DJ. Potential therapeutic applications of autophagy. *Nat Rev Drug Discov*. 2007;6(4):304–312.
15. Kim E, Goraksha-Hicks P, Li L, Neufeld TP, Guan KL. Regulation of TORC1 by Rag GTPases in nutrient response. *Nat Cell Biol*. 2008;10(8):935–945.
16. Sancak Y, et al. The Rag GTPases bind raptor and mediate amino acid signaling to mTORC1. *Science*. 2008;320(5882):1496–1501.
17. Efeyan A, et al. Regulation of mTORC1 by the Rag GTPases is necessary for neonatal autophagy and survival. *Nature*. 2013;493(7434):679–683.
18. Sun XJ, et al. Structure of the insulin receptor substrate IRS-1 defines a unique signal transduction protein. *Nature*. 1991;352(6330):73–77.
19. Sun XJ, et al. Role of IRS-2 in insulin and cytokine signalling. *Nature*. 1995;377(6545):173–177.
20. Cai D, Dhe-Paganon S, Melendez PA, Lee J, Shoelson SE. Two new substrates in insulin signaling, IRS5/DOK4 and IRS6/DOK5. *J Biol Chem*. 2003;278(28):25323–25330.
21. Lavan BE, Lane WS, Lienhard GE. The 60-kDa phosphotyrosine protein in insulin-treated adipocytes is a new member of the insulin receptor substrate family. *J Biol Chem*. 1997;272(17):11439–11443.
22. Lavan BE, Fantin VR, Chang ET, Lane WS, Keller SR, Lienhard GE. A novel 160-kDa phosphotyrosine protein in insulin-treated embryonic kidney cells is a new member of the insulin receptor substrate family. *J Biol Chem*. 1997;272(34):21403–21407.
23. Sesti G, Federici M, Hribal ML, Lauro D, Sbraccia P, Lauro R. Defects of the insulin receptor substrate (IRS) system in human metabolic disorders. *FASEB J*. 2001;15(12):2099–2111.
24. Uchida T, Myers MG, White MF. IRS-4 mediates protein kinase B signaling during insulin stimulation without promoting antiapoptosis. *Mol Cell Biol*. 2000;20(1):126–138.
25. White MF. Insulin signaling in health and disease. *Science*. 2003;302(5651):1710–1711.
26. Araki E, et al. Alternative pathway of insulin signalling in mice with targeted disruption of the IRS-1 gene. *Nature*. 1994;372(6502):186–190.
27. Tamemoto H, et al. Insulin resistance and growth retardation in mice lacking insulin receptor substrate-1. *Nature*. 1994;372(6502):182–186.
28. Pete G, et al. Postnatal growth responses to insulin-like growth factor I in insulin receptor substrate-1-deficient mice. *Endocrinology*. 1999;140(12):5478–5487.
29. Withers DJ, et al. Disruption of IRS-2 causes type 2 diabetes in mice. *Nature*. 1998;391(6670):900–904.
30. Sadagurski M, et al. IRS2 increases mitochondrial dysfunction and oxidative stress in a mouse model of Huntington disease. *J Clin Invest*. 2011; 121(10):4070–4081.
31. Kim J, Kundu M, Viollet B, Guan KL. AMPK and mTOR regulate autophagy through direct phosphorylation of Ulk1. *Nat Cell Biol*. 2011;13(2):132–141.
32. Lynch CJ. Role of leucine in the regulation of mTOR by amino acids: revelations from structure-activity studies. *J Nutr*. 2001;131(3):861S–865S.
33. Hara K, Yonezawa K, Weng QP, Kozlowski MT, Belham C, Avruch J. Amino acid sufficiency and mTOR regulate p70 S6 kinase and eIF-4E BP1 through a common effector mechanism. *J Biol Chem*. 1998;273(23):14484–14494.
34. Klionsky DJ, et al. Guidelines for the use and interpretation of assays for monitoring autophagy. *Autophagy*. 2012;8(4):445–544.
35. D'Antona G, et al. Branched-chain amino acid supplementation promotes survival and supports cardiac and skeletal muscle mitochondrial biogenesis in middle-aged mice. *Cell Metab*. 2010;12(4):362–372.
36. Qu X, et al. Promotion of tumorigenesis by heterozygous disruption of the beclin 1 autophagy gene. *J Clin Invest*. 2003;112(12):1809–1820.
37. Belke DD, et al. Insulin signaling coordinately regulates cardiac size, metabolism, and contractile protein isoform expression. *J Clin Invest*. 2002; 109(5):629–639.
38. Kim J, et al. Insulin-like growth factor I receptor signaling is required for exercise-induced cardiac hypertrophy. *Mol Endocrinol*. 2008;22(11):2531–2543.
39. Boudina S, et al. Contribution of impaired myocardial insulin signaling to mitochondrial dysfunction and oxidative stress in the heart. *Circulation*. 2009; 119(9):1272–1283.
40. Troncoso R, et al. Energy-preserving effects of IGF-1 antagonize starvation-induced cardiac autophagy. *Cardiovasc Res*. 2012;93(2):320–329.
41. Laustsen PG, et al. Essential role of insulin and insulin-like growth factor 1 receptor signaling in cardiac development and function. *Mol Cell Biol*. 2007; 27(5):1649–1664.
42. Bugger H, et al. Proteomic remodelling of mitochondrial oxidative pathways in pressure overload-induced heart failure. *Cardiovasc Res*. 2010; 85(2):376–384.
43. Zhang D, et al. MTORC1 regulates cardiac function and myocyte survival through 4E-BP1 inhibition in mice. *J Clin Invest*. 2010;120(8):2805–2816.
44. Zhu Y, et al. Mechanistic target of rapamycin (mtor) is essential for murine embryonic heart development and growth. *PLoS One*. 2013;8(1):e54221.
45. Des Rosiers C, Labarthe F, Lloyd SG, Chatham JC. Cardiac anaplerosis in health and disease: food for thought. *Cardiovasc Res*. 2011;90(2):210–219.
46. Dong XC, et al. Inactivation of hepatic Foxo1 by insulin signaling is required for adaptive nutrient homeostasis and endocrine growth regulation. *Cell Metab*. 2008;8(1):65–76.
47. Lin X, et al. Dysregulation of insulin receptor substrate 2 in beta cells and brain causes obesity and diabetes. *J Clin Invest*. 2004;114(7):908–916.
48. Abel ED, et al. Cardiac hypertrophy with preserved contractile function after selective deletion of GLUT4 from the heart. *J Clin Invest*. 1999;104(12):1703–1714.
49. Boudina S, et al. Mitochondrial energetics in the heart in obesity-related diabetes: direct evidence for increased uncoupled respiration and activation of uncoupling proteins. *Diabetes*. 2007; 56(10):2457–2466.
50. Dong X, Park S, Lin X, Copps K, Yi X, White MF. Irs1 and Irs2 signaling is essential for hepatic glucose homeostasis and systemic growth. *J Clin Invest*. 2006;116(1):101–114.
51. O'Neill BT, et al. A conserved role for phosphatidylinositol 3-kinase but not Akt signaling in mitochondrial adaptations that accompany physiological cardiac hypertrophy. *Cell Metab*. 2007;6(4):294–306.
52. Perry CN, Kyoi S, Hariharan N, Takagi H, Sadoshima J, Gottlieb RA. Novel methods for measuring cardiac autophagy in vivo. *Methods Enzymol*. 2009; 453:325–342.
53. Mandarim-de-Lacerda CA. Stereological tools in biomedical research. *An Acad Bras Cienc*. 2003; 75(4):469–486.
54. Bugger H, et al. Tissue-specific remodeling of the mitochondrial proteome in type 1 diabetic akita mice. *Diabetes*. 2009;58(9):1986–1997.
55. Riehle C, et al. PGC-1β deficiency accelerates the transition to heart failure in pressure overload hypertrophy. *Circ Res*. 2011;109(7):783–793.
56. Boudina S, Sena S, O'Neill BT, Tathireddy P, Young ME, Abel ED. Reduced mitochondrial oxidative capacity and increased mitochondrial uncoupling impair myocardial energetics in obesity. *Circulation*. 2005;112(17):2686–2695.